ICAS 2016
30th Congress of the International Council of the Aeronautical Sciences
DCC, Daejeon, Korea, September 25-30, 2016

DEVELOPMENT OF HIGH-ORDER AND HIGH-RESOLUTION SCHEMES FOR EFFICIENT SHOCK CAPTURING IN HIGH-SPEED FLOWS

Myeong-hwan Ahn*and Duck-joo Lee*
*** Department of Aerospace Engineering, KAIST, Daejeon, Korea**

Ketwords: *Compact-reconstruction, Optimization, Monotonicity-preserving*

Abstract

In this research, the high-order and high-resolution scheme was developed on the basis of conservative compact reconstruction method. The monotonicity preserving (MP) conditions which are known as shock capturing method were combined with the compact reconstruction. Furthermore, an optimization was adopted for achieving higher-resolution characteristics. In the scalar and Euler numerical tests, result in wave propagation and highly-oscillation problems were well-predicted by the optimized compact monotonicity preserving (OCMP) scheme which is developed in this paper6. In addition, discontinuities were captured well by using the MP conditions. Therefore, on the aspect of these advantages, the OCMP can be valuable scheme for the high-speed flows and aeroacoustics simulation.

1. Introduction

As the computer power have been grown up, computational fluid dynamics (CFD) become a very strong tool for investigating various flow physics without experiments which take much time and cost. In particular, the high-order method, which has low truncation error, have been developed to analyze complex fluid phenomena, such as shock, vortex and turbulent flow. However, for an aeroacoustics simulation, the numerical scheme that has not only high-order but also high- resolution characteristics is necessary. The high-resolution scheme enables to capture small acoustic pressure even in large size of grid region. The one of improving resolution methods is the compact scheme. For applications of aeroacoustics, various ‘compact schemes’ have been studied. The compact scheme uses an implicit form of flux derivative formula to get the high-order and high-resolution results.

Lele[1] introduced the spectral-like compact scheme. This scheme uses the compact formula with modified coefficients to improve the resolution. Kim and Lee[2] suggested an optimized high-order compact scheme (OHOC) by applying an optimization method which is similar with the dispersion-relation-preserving scheme[3]. These kinds of schemes are the finite difference methods (FDM). To prevent an oscillation across a discontinuity, the FDM mostly use artificial dissipation in the source term. However, the artificial dissipation makes the governing equation non-conservative form. Therefore, to get a robustness without introducing new term, the essentially non-oscillatory (ENO) [4] or weighted essentially non-oscillatory (WENO) method[5] have been coupled with the compact schemes. Deng and Maekawa [6] suggested the nonlinear compact scheme based on the FDM. This scheme uses numerical fluxes at the center of two node points. The ENO or WENO method is used when numerical fluxes are calculated. Zhang et al. [7] expanded the nonlinear compact schemes to higher orders to get more accurate results. Meanwhile, the hybrid scheme which couples the compact scheme and the essentially non-oscillatory method have been developed. The

'couple' means the compact form of equation works in a smooth region; but, the ENO or WENO serves in a discontinuity region. Pirozzoli [8] suggested the conservative-hybrid compact WENO scheme by applying the concept of compact scheme to the reconstruction process. Ren et al. [9] expanded it to characteristic domain. The hybrid schemes have been developed focusing on stability in the high-speed flow conditions which contain the shock. However, in a discontinuity region, high resolution characteristic cannot be maintained because of switching to the WENO. In order to solve this problem, the compact-reconstruction WENO (CRWENO) scheme was proposed by Ghosh and Baeder[10]. Because the compact reconstruction contains all weighting coefficients, a solution can keep high-resolution characteristic even across a discontinuity.

On the other hand, the monotonicity preserving (MP) scheme[11] also was suggested for the compact schemes instead of the WENO. The WENO controls a discontinuity with only interpolation and weighting; but, it attenuates solutions even in a smooth region. However, the MP conditions do not dissipate solution and capture shock clearly. Huynh who developed the MP scheme suggested an implicit reconstruction with MP conditions and verified numerically in the scalar equation [12] (not up to the Euler).

In this paper, based on the compact improved-wave-resolution method, we extend this idea to the Euler equation, and developed optimized compact reconstructions with MP conditions also. The usage of the MP was expected to makes result more accurate at the extrema and discontinuity. Moreover, by using optimized coefficients, the compact reconstructions achieve a high-resolution characteristics in comparison with other methods.

2. Numerical method

2.1 Governing equation and discretization

In order to simulate the compressible flow, the continuity, momentum and energy equations are should be solved numerically. The governing equation is given by,

$$\frac{\partial \boldsymbol{U}}{\partial t} + \operatorname{div} \boldsymbol{F} = 0 \qquad (1)$$

Each vector of $\boldsymbol{U}$ and $\operatorname{div}\boldsymbol{F}$ means the conservative variable and flux derivative terms, respectively. When the dimension of system is N; then, $\operatorname{div}\boldsymbol{F}$ can be expressed as follows :

$$\operatorname{div}\boldsymbol{F} = \frac{\partial F_1}{\partial x_1} + \frac{\partial F_2}{\partial x_2} + \ldots + \frac{\partial F_N}{\partial x_N} \qquad (2)$$

The $\operatorname{div}\boldsymbol{F}$ can be changed to the jacobian and $\operatorname{div}\boldsymbol{U}$. When the transformed term is digonalized, a numerical scheme can deal with the governing equation robustly: This form of equation is expressed with characteristic variables. We discuss about it in the section 2.5.

To solve the governing equation (1) in space, it should be expressed in the semi-discretized form. The equation is obtained by integrating for an arbitrary cell :

$$\frac{\partial}{\partial t}\bar{\boldsymbol{u}}(x_j,t) + \frac{\boldsymbol{h}(x_{j+1/2},t) - \boldsymbol{h}(x_{j-1/2},t)}{\Delta x} = 0 \qquad (3)$$

$$\frac{\boldsymbol{h}(x_{j+1/2},\mathrm{t}) - \boldsymbol{h}(x_{j-1/2},\mathrm{t})}{\Delta x} = \frac{\hat{\mathbf{f}}_{j+1/2} - \hat{\mathbf{f}}_{j-1/2}}{\Delta x} + O(\Delta x^r) \qquad (4)$$

The averaged value is given by,

$$\bar{\boldsymbol{u}}(x_j,t) = \frac{\int_{j-1/2}^{j+1/2} \boldsymbol{u}(x,t)}{\Delta x} \qquad (5)$$

The order of numerical flux $\hat{f}$ in equation (4) determine the spatial order of scheme.

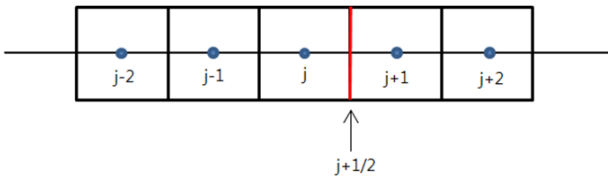

Fig. 1. Schematic for fifth-order explicit reconstruction (explicit form)

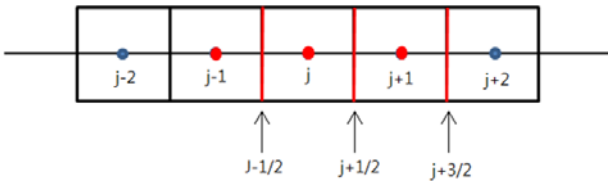

Fig. 2. Schematic for fifth-order compact reconstruction (implicit form)

2.2 High-order and high-resolution method

We started from simple wave equation to understanding a reconstruction because the hyperbolic system of governing equation is based on the propagation of characteristic values. In this section, all reconstructions are derived in right-going wave situation.

How well define the numerical flux terms is important. The simplest way to get flux values is only j and j-1 cells participate in the reconstruction step. If more than one cell are used, the spatial-order can be increased. For example, using five cells makes fifth-spatial order.

$$\hat{f}_{j+1/2} = \frac{1}{30} f_{j-2} - \frac{13}{60} f_{j-1} + \frac{47}{60} f_j + \frac{27}{60} f_{j+1} - \frac{1}{20} f_{j+2} \tag{6}$$

The WENO5 and MP5 are based on the formula (6). This reconstruction decides one numerical flux directly from five cell average values explicitly (Figure 1). Each coefficients can be derived from the Taylor series expansion.

Meanwhile, S. Pirozzoli [8] suggested the implicit form of reconstruction from the concept of the compact scheme (Figure 2). This reconstruction also has fifth-spatial order accuracy, but it has higher resolution than the explicit reconstruction (6).

$$\begin{aligned} &\frac{3}{10}\hat{f}_{j-1/2} + \frac{3}{5}\hat{f}_{j-3} + \frac{1}{10}\hat{f}_{j-2} \\ &\quad = \frac{1}{30} f_{j-1} + \frac{19}{30} f_j + \frac{1}{3} f_{j+1} \end{aligned} \tag{7}$$

The compact reconstruction improves both dispersion and dissipation errors. For calculating fluxes using reconstruction (7), a tri-diagonal solver must be used such as Thomas algorithm.

2.3 Optimization

In terms of continual study for the high-resolution method, new forms of reconstruction which have higher resolution than the fifth-order compact reconstruction (7) were derived. First of all, we added another stencils to the compact reconstruction (7) as below,

$$\begin{aligned} &a\cdot\hat{f}_{j-1/2} + b\cdot\hat{f}_{j+1/2} + c\cdot\hat{f}_{j+3/2} \\ &= d\cdot f_{j-2} + e\cdot f_{j-1} + g\cdot f_j + h\cdot f_{j+1} + k\cdot f_{j+2} \end{aligned} \tag{8}$$

$$\begin{aligned} &a\cdot\hat{f}_{j-3/2} + b\cdot\hat{f}_{j-1/2} + c\cdot\hat{f}_{j+1/2} + d\cdot\hat{f}_{j+3/2} + e\cdot\hat{f}_{j+5/2} \\ &= g\cdot f_{j-2} + h\cdot f_{j-1} + k\cdot f_j + l\cdot f_{j+1} + m\cdot f_{j+2} \end{aligned} \tag{9}$$

In order to get unknowns, the optimization suggested by Kim and Lee [2] was applied. Reconstructions (8) and (9) should be moved to the frequency domain by using the Fourier transform to be optimized. After transformation, compact reconstructions were converted into the modified wavenumber.

$$\begin{aligned} \bar{\kappa}(\kappa) = &\frac{A(\kappa)C(\kappa) + B(\kappa)D(\kappa)}{[A(\kappa)]^2 + [B(\kappa)]^2} \\ &+ i\frac{A(\kappa)D(\kappa) - B(\kappa)C(\kappa)}{[A(\kappa)]^2 + [B(\kappa)]^2} \end{aligned} \tag{10}$$

there are four functions in the modified wavenumber as,

$$\begin{aligned} A(\kappa) = &\, a\cos(2\kappa) + b\cos(\kappa) + c \\ &+ d\cos(\kappa) + e\cos(2\kappa) \end{aligned} \tag{11}$$

$$B(\kappa) = -a\sin(2\kappa) - b\sin(\kappa) + d\sin(\kappa) + e\sin(2\kappa) \tag{12}$$

$$C(\kappa) = g\sin(3\kappa) + (h-g)\sin(2\kappa) + (k-h)\sin(\kappa) + (l-m)\sin(\kappa) + m\sin(2\kappa) \tag{13}$$

$$D(\kappa) = g\cos(3\kappa) + (h-g)\cos(2\kappa) + (k-h)\cos(\kappa) + (l-k) + (m-l)\cos(\kappa) - m\cos(2\kappa) \tag{14}$$

There are real and imaginary parts in the modified wavenumber. Each part showes the dispersion and dissipation error, respectively. High-resolution means that a real part is closed to the wavenumber, and an imaginary part is reduced to zero. Kim and Lee [2] suggested the integrated error to define the discrepancy between the exact and numerical value,

$$E \equiv \int_0^{r\pi} \left|\overline{\kappa} - \kappa\right|^2 W(\kappa)\, d\kappa = \int_0^{r\pi} \left\{ \left[\mathrm{Re}(\overline{\kappa}) - \kappa \right]^2 + \left[\mathrm{Im}(\overline{\kappa}) \right]^2 \right\} W(\kappa)\, d\kappa \tag{15}$$

Where r is an integration range. The weighting function was given as,

$$W(\kappa) = \left\{ \sqrt{[A(\kappa)]^2 + [B(\kappa)]^2}\, e^{\kappa} \right\}^2 \tag{16}$$

The weighting function enables an error value is weighted on the high-wavenumber part. Finally, the error was differentiated to minimize the integrated error (15).

$$\frac{\partial \mathrm{E}}{\partial \Omega} = 0 \quad (\Omega \text{ can be } a, b, c, d, e, g, h, k) \tag{17}$$

To get unknowns, we needed the same number of conditions as that of coefficients; thus, eight equations were used for equation (8), and ten equations were used for equation (9). We derived fifth-order schemes. That means, the conditions from the Taylor series expansion were used up to fifth-order. The other equations came from minimized error conditions (17). As a result of solving equation, coefficients in equation (8) were,

$$\begin{aligned} a &= 0.2857429393 \quad b = 0.5692958015 \\ c &= 0.1449612591 \quad d = -0.0025586832 \\ e &= 0.0463092557 \quad g = 0.5658914446 \\ h &= 0.3803057563 \quad k = 0.0100522263 \end{aligned} \tag{18}$$

And those in equation (9) were,

$$\begin{aligned} a &= 0.0423271107 \quad b = 0.3166585964 \\ c &= 0.4689952087 \quad d = 0.1630509037 \\ e &= 0.0089681802 \quad g = 0.0019067568 \\ h &= 0.1319816987 \quad k = 0.4887185819 \\ l &= 0.3393162663 \quad m = 0.0380766961 \end{aligned} \tag{19}$$

2.4 Monotonicity preserving (MP) conditions

After the numerical fluxes are determined by the compact reconstruction, the Gibb's phenomena can occur across a discontinuity.

In this study, the monotonicity preserving (MP) conditions known as producing more accurate solution than the WENO were used for resolving the Gibb'b phenomena. Suresh and Huynh [11] suggested the conditions as follow,

$$\begin{aligned} v^{OR} &= \hat{f}_{j+1/2} \\ v^{MD} &= \frac{1}{2}(f_j + f_{j+1}) - \frac{1}{2} d^{MM}_{j+1/2} \\ v^{UL} &= f_j + \alpha(f_j + f_{j-1}) \\ v^{LC} &= f_j + \frac{1}{2}(f_j - f_{j-1}) + \frac{4}{3} d^{MM}_{j-1/2}\ , \end{aligned} \tag{20}$$

$$\begin{aligned} v^{\min} &= \max[\min(f_j, f_{j+1,} v^{MD}), \min(f_j, v^{UL} v^{LC} \\ v^{\max} &= \min[\max(f_j, f_{j+1,} v^{MD}), \max(f_j, v^{UL} v^{L(\\ v^{MP} &= \mathrm{median}[v^{OR}, v^{\min}, v^{\max}] \end{aligned} \tag{21}$$

$$\begin{aligned} d^{MM}_{j+1/2} &= \mathrm{minmod}(d_j, d_{j+1}) \\ d_j &= f_{j-1} + f_{j+1} - 2 f_j\ . \end{aligned} \tag{22}$$

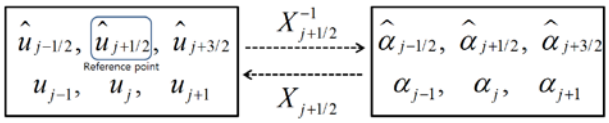

Fig. 3. Conservative and characteristic variables

Where $\alpha = 4$. The v^{MP} is the final numerical flux controlled by the MP conditions.

2.5 Extension to Euler equation

All reconstructions in section 3 were derived on the scalar equation. Now, we extend the compact and optimized compact reconstructions to the Euler equation. The one-dimensional Euler equation is given by,

$$\frac{\partial \boldsymbol{U}}{\partial t} + \frac{\partial \boldsymbol{F}}{\partial x} = 0 \tag{23}$$

Here, $\boldsymbol{U}$ and $\boldsymbol{F}$ vectors contain conservation, momentum, and energy equations.

$$\boldsymbol{U} = \begin{bmatrix} \rho \\ \rho u \\ e \end{bmatrix}; \qquad \boldsymbol{F} = \begin{bmatrix} \rho u \\ \rho u^2 + p \\ (e+p)u \end{bmatrix} \tag{24}$$

As can be seen in Figure 3, the decoupled system of equation can be derived after multiplying left-eigenvector to the Euler equation.

$$X^{-1} = \begin{bmatrix} \frac{(\gamma-1)u^2}{4a^2} + \frac{u}{2a} & -\frac{(\gamma-1)u}{2a^2} - \frac{1}{2a} & \frac{\gamma-1}{2a^2} \\ 1 - \frac{(\gamma-1)u^2}{2a^2} & \frac{(\gamma-1)u}{a^2} & -\frac{\gamma-1}{a^2} \\ \frac{(\gamma-1)u^2}{4a^2} - \frac{u}{2a} & -\frac{(\gamma-1)u}{2a^2} + \frac{1}{2a} & \frac{\gamma-1}{2a^2} \end{bmatrix} \tag{24}$$

$$\frac{\partial \boldsymbol{\alpha}}{\partial t} + \boldsymbol{\Lambda}\frac{\partial \boldsymbol{\alpha}}{\partial x} = 0 \tag{25}$$

$$\boldsymbol{\alpha} = \boldsymbol{X}^{-1}\mathbf{u} \tag{26}$$

Variables in the left eigenvector (24) were calculated from the roe average value. The equation (25) is the characteristic form of the 1-D Euler equation, and $\boldsymbol{\alpha}$ is the characteristic vector. This equation can be separated into three decoupled equations; therefore, the reconstruction step can be adapted to the Euler equation with more physical sense.

Finally, after characteristic values had been reconstructed in each direction, the Roe scheme [13] was used to get final fluxes.

$$\begin{aligned} \hat{\mathbf{f}}_{j+1/2} = & \frac{1}{2}\left(\hat{\mathbf{f}}^{L}_{j+1/2} + \hat{\mathbf{f}}^{R}_{j+1/2}\right) \\ & - \frac{1}{2}\left|\hat{A}\left(\hat{\mathbf{u}}^{L}_{j+1/2}, \hat{\mathbf{u}}^{R}_{j+1/2}\right)\right|\left(\hat{\mathbf{f}}^{L}_{j+1/2} + \hat{\mathbf{f}}^{R}_{j+1/2}\right) \end{aligned} \tag{27}$$

Where L and R means left- and right-biased reconstructed value, respectively.

2.6 Time integration

A time step integration was conducted after the spatial step was finished. In this research, the 3rd order total variation diminishing Runge-Kutta method (TVDRK3) was used. This method is more stable than classical Runge-Kutta method, especially in the hyperbolic type of equation. Three stages of integration are expressed as,

$$\begin{aligned} v^{(0)} &= u^n \\ v^{(1)} &= v^{(0)} + \Delta t\, L(v^{(0)}) \\ v^{(2)} &= \frac{3}{4}v^{(0)} + \frac{1}{4}\left[v^{(1)} + \Delta t\, L(v^{(1)})\right] \\ v^{(3)} &= \frac{1}{3}v^{(0)} + \frac{2}{3}\left[v^{(2)} + \Delta t\, L(v^{(2)})\right] \\ u^{n+1} &= v^{(3)} \end{aligned} \tag{28}$$

3. Results

3.1 Fourier analysis

The resolution of reconstruction can be checked analytically by using the Fourier analysis. We already derived the modified wavenumber (10) in section 2. Each real and

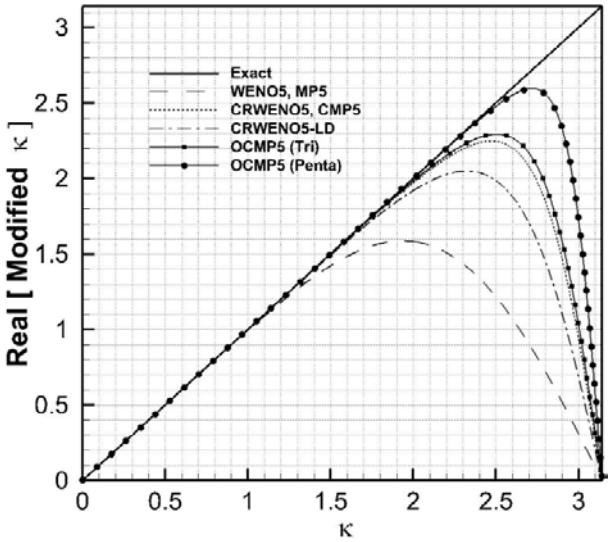

Fig. 4. Modified wavenumber : Real part

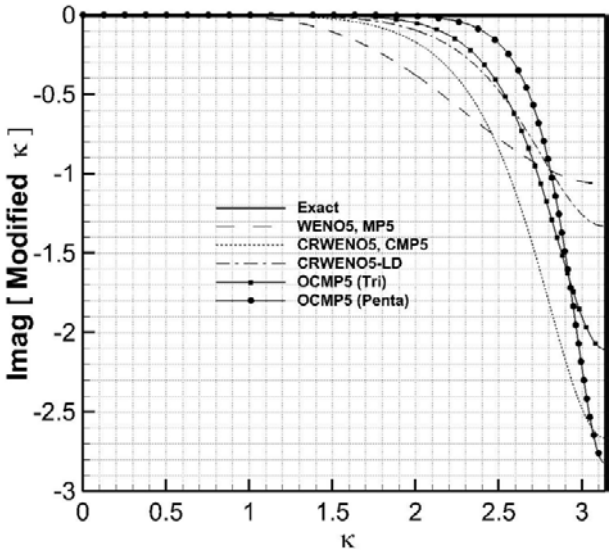

Fig. 5. Modified wavenumber : Imaginary part

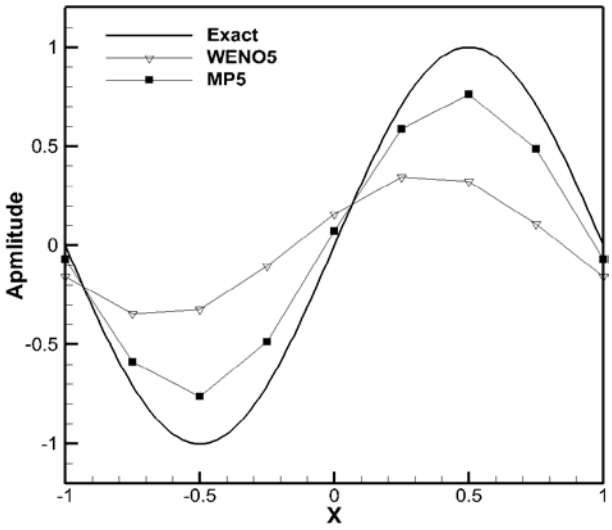

Fig. 6. The results of sine wave propagation (N=8, after 10 period)

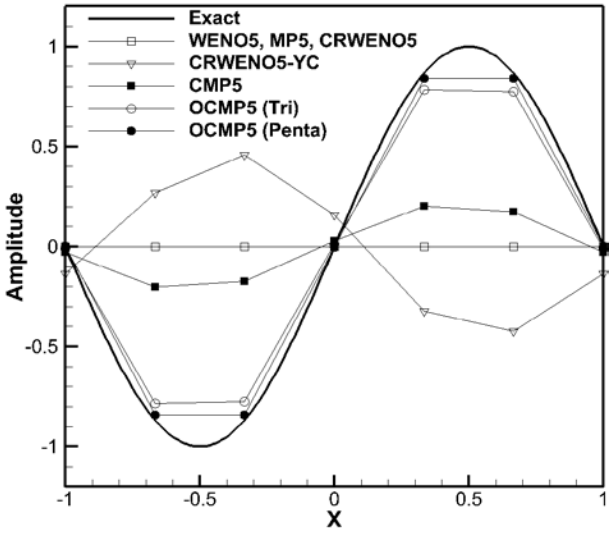

Fig. 7. The results of sine wave propagation (N=6, after 100 period)

imaginary part in the modified wavenumber can be plotted as the wavenumber to figure out the resolution characteristics of scheme.

Prior to comparisons, terminologies for present schemes need to be explain. The CMP5 means the fifth-order compact reconstruction (7) coupled with the MP conditions. For optimized schemes, 'O' is placed in front of the name of scheme. 'Tri' is the tridiagonal form of reconstruction (8), and 'Penta' means the pentadiagonal form of construction (9). The resolutions of the WENO, CRWENO, and CRWENO-LD [10] are presented as references.

Figure 4 shows the real part of resolution, and Figure 5 presents the imaginary part of resolution. As can be seen in Figures, the compact reconstruction can increase the resolution significantly. Furthermore, the usage of 5^{th} order optimized compact reconstruction (8) and (9) much improve the resolution than fifth-order compact reconstruction.

Above comparisons are conducted by using analytical way. Numerical verifications are presented in the next section.

3.2 Sine wave propagation problem

The scheme which can capture far propagating acoustic wave with fewer cells has higher resolution characteristics. In this section, the sine wave propagation problem was solved with periodic boundary condition.

Equation (1) was set up as one-dimension and expressed in the scalar form as below,

$$\frac{\partial u}{\partial t}+\frac{\partial f}{\partial x}=0\ ;\quad f=u(x,t) \tag{29}$$

$$u_0(x)=Sin(\pi x).\quad (-1\le x\le 1) \tag{30}$$

The governing equation (29) indicates the wave equation. The speed of sound is one. Simulation conditions were : a CFL number was 0.1, and initial condition was sine shape wave (30).

Figure 6 shows the result of the WENO5 and MP5 schemes with eight cells. As the MP conditions do not distort a reconstruction in a smooth region, the MP5 has more accurate result than the WENO5 even though they use same explicit reconstruction. This merit is also effective on the compact reconstruction. Figure 7 displays the result of various schemes with six cells. For a clear comparison, long propagating condition (100 period) was chosen. In this tough condition, we did not get meaningful data using the WENO5 and MP5 because truncation error was so large. Note that even though the compact reconstruction was used, the solution of the CRWENO5 is almost dissipated because of weightings, whereas the CMP5 still has the sine shape. The weighting dissipation of CRWENO5 can be improved by the energy stable WENO method[14] (CRWENO5-YC); but, it has large dispersive error. However, with the optimized compact reconstruction, the OCMP5 (Tri) and OCMP5 (Penta) have very accurate result.

The result tendency of the numerical test

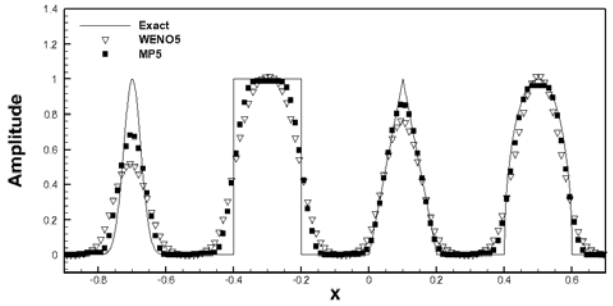

(a)

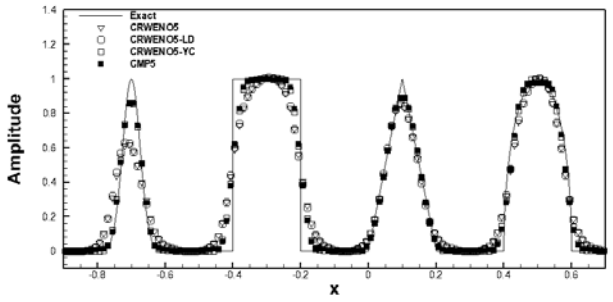

(b)

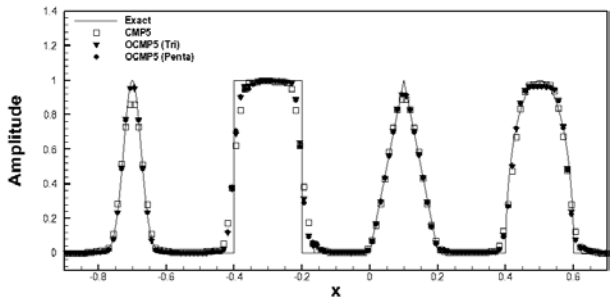

(c)

Fig. 8. The results of the propagation of various shape waves (N=160)

correspond with the analytical results in the previous section.

3.3 The propagation of various shape waves

In this section, waves propagation problem including discontinuities is presented. To simulate this case, a limiting process such as the WENO or MP conditions must be included in the numerical scheme to prevent oscillation near a discontinuity.

A CFL number was chosen as 0.1. Total cell number was 160, and the initial condition were composed of four kinds of wave: an exponential, square, triangular and parabola shapes. Detail informations as follow,

$$
\begin{aligned}
u_0(x) &= e^{-\log 2\frac{(x+0.7)^2}{0.0009}} && (-0.8 \le x \le -0.6) \\
&= 1 && (-0.4 \le x \le -0.2) \\
&= 1-|10(x-0.1)| && (0 \le x \le 0.2) \\
&= \left[1-100(x-0.5)^2\right]^{1/2} && (0.4 \le x \le 0.6) \\
&= 0 && \text{Otherwise}
\end{aligned} \tag{31}
$$

Figure 8(a) demonstrates the solution of non-compact methods: the WENO5 and MP5. As we expected, the MP5 shows good performance on all wave shapes. Across discontinuities, the MP conditions captured them well. The reason for better accuracy in smooth regions follows the same manner as the sine wave propagation. Figure 8(b) shows compact reconstruction schemes combined with the WENO or MP method. All schemes give an improved solution compared with the non-compact method. By adapting the energy stable WENO method, the CRWENO5-YC has similar result with the CMP5. Note that the MP conditions still activate well with the compact reconstruction. The performance of the optimized schemes developed in this paper are presented in Figure 8(c). Both optimized tri- and penta-diagonal schemes almost coincident with the exact solution, particularly in peak region.

3.4 Shock-entropy wave interaction problem

An interaction between Mach 3 shock and continual entropy wave was discussed using different schemes. From this problem, we can investigate how accurately numerical methods simulate the compressible-turbulence flows. The initial condition was as below,

$$
\rho,\ u,\ p = \begin{cases} \dfrac{27}{7},\ \dfrac{4\sqrt{35}}{9},\ \dfrac{31}{3} & (x < -4.0) \\ 1+\dfrac{1}{5}\sin 5x,\ 0,\ 1 & (x \ge -4.0) \end{cases} \tag{31}
$$

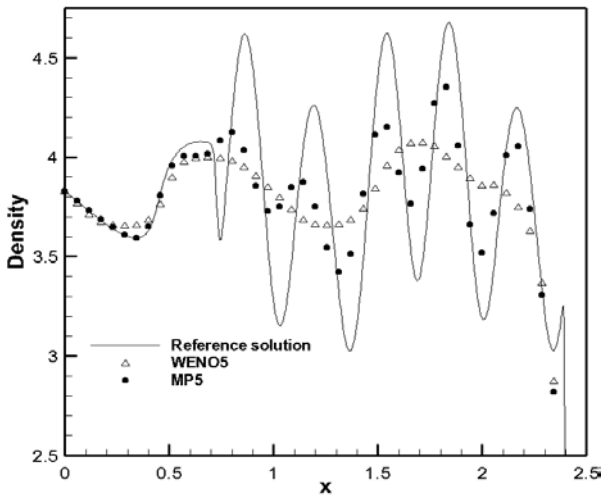

(a)

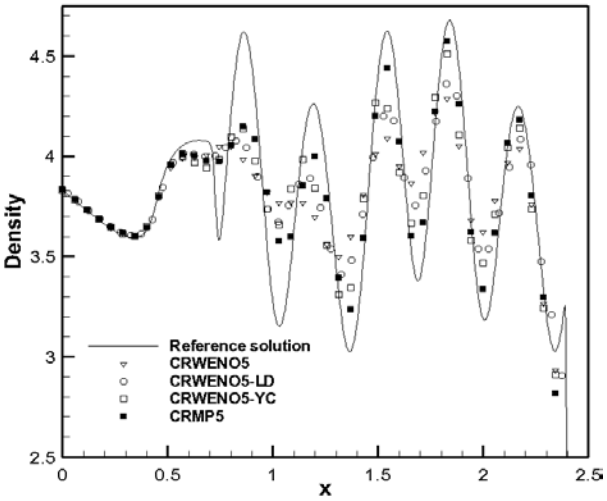

(b)

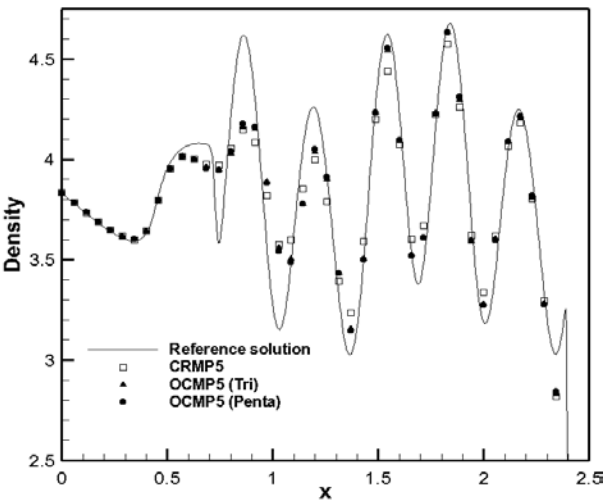

(c)

Fig. 9. The results of the shock-entropy wave interaction (N=175)

A CFL number was same as in the previous condition was imposed at both ends. Then, results after 1.8 second were collected. We set up the number of cells as 175 for comparison (for 6cells on a wave in high-frequency region).

As there is no exact solution in the shock-entropy wave interaction problem, reference data from fine grid simulation is necessary. In order to get a reference, the result calculated by the CRWENO5 with 2000 cells was chosen.

In a high-frequency dominant region, the advantage of the MP5 comes out more clearly. As can be seen in Figure 9(a), the WENO5 has large dissipation error, whereas the MP5 follows the oscillation behavior. When both methods were combined with the compact reconstruction, in Figure 9(b), there is also large discrepancy between the CRWENO5-YC and CMP5, unlike previous tests. It means that reconstruction is sensitively affected by limiting process especially in a high-frequency region. In Figure 9(c) as the final comparison, the OCMP5(Tri) and OCMP5 (Penta) which use more stencil and optimized coefficients have more accurate result than the CMP5 .

4. Conclusion

In this paper, the optimized compact monotonicity preserving (OCMP) scheme was developed by adapting the optimization to the compact scheme, and by combining reconstruction with the MP conditions. The development procedure was focused on not only a high-accurate shock capturing ability but also high-resolution characteristic to calculate strong non-linear acoustics.

1. The advantage of the MP conditions is capturing shock well, and enables maintaining the order of accuracy when the MP conditions does not activate. This merit was effective when the MP conditions were combined with the compact reconstruction. In numerical comparisons, the CMP5 had better accuracy than the other WENO-series schemes on scalar and Euler equation.

2. The numerical tests on scalar equation showed that optimized schemes had better accuracy than other methods because of the highest-resolution. The result of the Euler equation also presented that the OCRMP5 schemes (tri- and penta-diagonal forms) coincided well with both the shock and highly-oscillatory region. These characteristics of present scheme enable that a generated sound from shock and vortex flow propagated to a far-field accurately

Acknowledgments

This research was supported by the Space Core Technology Development program (Grant No. NRF-2014M1A3A3A02034837) through the NRF (National Research Foundation of Korea) funded by the Ministry of Science, ICT.

References

[1] Lele S. K. Compact finite difference schemes with spectral-like resolution. *Journal of Computational Physics* Vol. 103, No. 1, pp 16-42, 1992.

[2] Kim J. W. and Lee D. J. Development of compact finite difference schemes optimized for computational aeroacoustics. Master Thesis, KAIST, 1996

[3] Tam C. K. W. and Webb J. C. Dispersion-Relation-Preserving finite difference schemes for computational acoustics. *Journal of Computational Physics*, Vol. 107, No. 2, pp 262-281, 1993

[4] Harten A. and Osher S. Uniformly high-order accurate non-oscillatory schemes I, *SIAM Journal of Numerical Analysis*, Vol. 24, pp 279-309, 1987

[5] Liu X. D, Osher S. and Chan T. Weighted essentially non-oscillatory schemes. *Journal of Computational Physics*, Vol. 115, No. 1, pp 200-212, 1994

[6] Deng X. and Maekawa H. Compact high-order accurate nonlinear schemes. *Journal of Computational Physics*, Vol. 130, No. 1, pp 77-91, 1997

[7] Zhang S, Jiang S. and Shu C.-W. Development of nonlinear weighted compact schemes with increasingly higher order accuracy. *Journal of Computational Physics*, Vol. 227, Vol. 15, pp 7294-7321, 2008

[8] Pirozzoli S. Conservative hybrid compact-WENO schemes for shock-turbulence interaction. *Journal of Computational Physics*, Vol. 178, No. 1, pp 81-117, 2002

[9] Ren Y, Liu M. and Zhang H. A characteristic-wise hybrid compact-WENO scheme for solving hyperbolic conservation laws. *Journal of Computational Physics,* No. 192, No. 2, pp 365-386, 2003
[10] Ghosh D. and Baeder D. Compact Reconstruction Schemes with Weighted ENO Limiting for Hyperbolic Conservation Laws. *SIAM Journal on Scientific Computing*, Vol. 34, No. 3, pp A1678-A1706, 2012
[11] Suresh A. and Huynh H. T. Accurate monotonicity-preserving schemes with Runge-Kutta time stepping. *Journal of Computational Physics*, Vol. 136, No. 1, pp 83-99, 1997
[12] Huynh H. T. Schemes and constraints for advection. *Fifteenth International Conference on Numerical Methods in Fluid Dynamics Lecture Notes in Physics*, Vol. **490**, pp 498-503, 1997
[13]Roe P. L. Approximate Riemann solvers, parameter vectors and difference schemes. *Journal of Computational Physics*, Vol. 43**,** No. 2 **,** pp 357-372, 1981
[14] Yamaleev N. K. and Carpenter M. H. Third-order energy stable WENO scheme. *Journal of Computational Physics*, Vol. 228, No. 8, pp 3025-3047, 2009

Copyright Statement